Int. J. Electrochem. Sci., 12 **(2017)** 9542 – 9554, doi: 10.20964/2017.10.32

International Journal of
ELECTROCHEMICAL
SCIENCE
www.electrochemsci.org

Corrosion Behavior of the Al_2Cu Intermetallic Compound and Coupled Al_2Cu/Al

Herong Zhou[1,2,*], *Wang Yao*[2], *Cuiwei Du*[3], *Shupeng Song*[2], *Run Wu*[2]

[1] The State Key Laboratory of Refactories and Metallurgy, Wuhan University of Science and Technology, Wuhan, 430081, PR China;
[2] School of Material and Metallurgy, Wuhan University of Science and Technology, Wuhan, 430081, PR China;
[3] University of Science and Technology Beijing, Beijing, 100083, PR China;
[*]E-mail: zhouhr_9@163.com

Received: 8 April 2017 / *Accepted:* 25 July 2017 / *Published:* 12 September 2017

The corrosion behavior of intermetallic Al_2Cu has been investigated using polarization, electrochemical impedance spectroscopy (EIS), scanning kelvin probe (SKP), local electrochemical impedance (LEIS) and scanning electron microscopy. The corrosion potential of intermetallic Al_2Cu is measured to be -473.04 mV in 0.1 M Na_2SO_4 solution with pH 4.3. The highest corrosion rate over the immersing time between 0 and 96 h is observed at 48 h according to the EIS results. The potential results of coupled Al_2Cu/Al reveal that the Al_2Cu potential becomes positive during the immersion time and is higher than that of pure Al near the interface. The local impedance value of intermetallic Al_2Cu increases greatly and is higher than that of pure Al. Thus, the corrosion degree of pure Al is more severe than that of intermetallic Al_2Cu because of the galvanic corrosion of coupled Al_2Cu/Al.

Keywords: intermetallic Al_2Cu； corrosion behavior; EIS； SKP； LEIS

1. INTRODUCTION

The 2A12 alloy has been widely used in the industry due to its high strength and yield ratio and economic efficiency compared to the other Al–Mg–Cu alloy systems. However, 2A12 alloy is easily susceptible to local corrosion in the industrial or marine atmospheric environment because of the high number amount of structural defects and intermetallic compounds. Intermetallic compounds such as Al_2Cu, Al_2CuMg, and $(Al,Cu)_6Mn$ improve the material mechanical properties of the 2A12 alloy [1-3] but also lead to pits and intergranular corrosion because of the difference in the potential between the intermetallic and the aluminum (Al) matrix [4-6].

Intermetallic Al_2Cu is an important intermetallic compound that greatly influences the corrosion behavior of the 2A12 alloy. Unfortunately, it is very difficult to continuously investigate the corrosion

behavior and its mechanism for the Al_2Cu intermetallic compound in bulk Al alloy using electrochemical methods because of the small size of intermetallic Al_2Cu [7-21]. SEM micrographs and the potentials of intermetallic Al_2Cu in the AA2017 alloy have been studied [7]. The coarse Al_2Cu crystallite had a strong influence on the cathodic process of the 2024 alloy and was related to the pitting susceptibility [8]. The Al_2Cu phase in the 2024 alloy was very important for micro-corrosion and local corrosion according to the results obtained by F. M. Queiroz [10]. The selective dissolution of Al in the θ (Al_2Cu) phase resulted in a porous copper-rich remnant and the de-alloying of the θ phase. The de-alloying in the θ phase could preferentially occur below the sample surface and was related to the local low pH environment [12]. A. C. Vieira [18] has considered effect of the Al_2Cu phase size on the mass transport dependent kinetics of oxygen reduction. On the other hand, smelting the same component materials as those in the intermetallic is a common approach for the study of the corrosion resistance of intermetallics [21-24]. The Al_2Cu phase was found to be the origin of corrosion and promoted the corrosion in Al - copper complex structure material, with the copper content showing little effect on the open circuit potential according to the results of W. R. Osorio [21]. The bulk Al-Cu alloy improved the corrosion resistance of the alloy as seen by polarization and electrochemical impendence spectrum experiments [22]. However, the method for studying the corrosion behavior of molten intermetallic Al_2Cu is rarely used in a certain environmental medium.

Galvanic corrosion in an Al alloy has been studied [24-26]. The authors had developed a finite-element model in order to study the influence of the microstructure on the micro-galvanic corrosion of Al alloys [24]. The influence of cerium cinnamate on the galvanic corrosion of the coupled Al_2Cu and Al was studied and cerium cinnamate played an inhibitory role in the coupling corrosion of Al_2Cu-Al on the basis of cerium oxide/hydroxide production [25]. However, the corrosion behavior and mechanism of intermetallic Al_2Cu are still unclear due to the influence of different structures in the material.

Environment pollution has very important influence on the corrosion behavior of Al alloys. Industrial environmental pollution media such as sulfur dioxide, haze, and ash are found in high concentrations in some economically developed regions or big cities in China. In particular, sulfur dioxide shows one of the strongest effects on the corrosion of Al materials such as the 2A12 alloy. The Jiangjin district is a typical location for studying the industrial atmospheric pollution of metallic materials in China with a perfect atmosphere monitoring system available for such studies. The 2A12 alloy is widely used in many fields such as high-speed rail, aircraft, and equipment and its corrosion behavior directly affects the service life of many types of equipment. The corrosion behavior and mechanism of intermetallic Al_2Cu in the 2A12 alloy need to be studied in detail in the industrial pollution atmospheric environment in the Jiangjin district in China.

2. EXPERIMENTAL

2.1. Experimental material

Pure Al (100% α phase), intermetallic Al_2Cu and coupled Al_2Cu/Al were used in the experiments. The bulk form of intermetallic Al_2Cu was prepared from commercially pure Al (99.99%) and Cu (99.95%). The alloy was synthesized by combining the relevant proportions of Al (45.96 *wt.*%)

and Cu (54.04 *wt.*%) in a crucible. The process involved blending raw materials according to the Al-Cu phase diagram of the ratio, smelting these metal materials in the intermediate frequency vacuum induction furnace (version ZG001), pouring into the die, cooling by water, and then acquiring and annealing the cast ingot. The Al_2Cu intermetallic compound material was cut into the sample with the dimensions of 10 mm×10 mm×5 mm by line cutting for the test. Pure Al with the thickness of approximately 5 mm was deposited on the surface of the Al_2Cu sample with the dimensions of 10 mm×10 mm×5 mm in order to simulate the couple of intermetallic Al_2Cu and Al matrix (α-Al) in the 2A12 alloy. Thus, coupled Al_2Cu/Al is prepared for tests (Fig. 1).

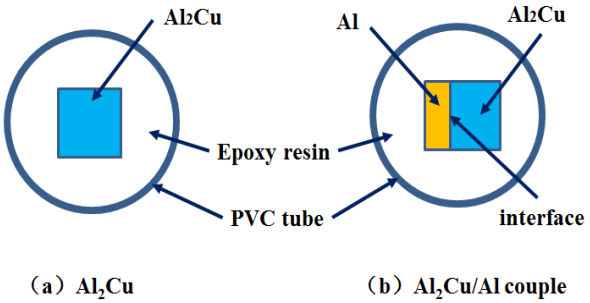

Figure 1. Schematic representation of Al_2Cu (a) and Al_2Cu /Al couple electrode (b) model

The electrode samples for electrochemical testing were sealed by epoxy, leaving one of the surfaces with 1 cm×1 cm area open to the air to serve as the working electrode. Prior to the experiments, the exposed surface was sanded and polished by diamond paste, then degreased in acetone, and finally washed by distilled water and dried with a blower.

2.2 Polarization tests and EIS measurements

Polarization and EIS tests were performed on a multi-channel electrochemical workstation (model VMP3) using a three-electrode system. To study the SO_2 corrosion behavior of intermetallic Al_2Cu in the Jiangjin district in China, the SO_2 concentration in the Jiangjin district is used for data support to prepare the simulation solution. The simulation solution was 0.1 M Na_2SO_4 with pH 4.3. The polarization curves were determined by increasing the potential from about −1.0 V (SCE) to +0.2 V (SCE) related to the open-circuit potential at the 0.166 mV/s scan rate. The working electrode was intermetallic Al_2Cu or pure Al, with Pt wire as the counter electrode and a saturated calomel electrode as the reference electrode.

The electrode samples of the Al_2Cu intermetallic compound used for the EIS tests were immersed in 0.1 M Na_2SO_4 solution with pH 4.3 for approximately 96 h. EIS measurements were always conducted from high frequency to low frequency with the frequency range of 100 kHz–10 mHz at 20±2 ℃. The amplitude of the used sinusoidal signal was 5 mV relative to the open-circuit potential. The impedance experimental data were analyzed in terms of an appropriate equivalent circuit using the ZSimpWin program. The parameters were determined by the simulation.

2.3 SKP and LEIS tests

A Al_2Cu/Al couple specimen was immersed in 0.1 M Na_2SO_4 solution with pH 4.3 for approximately 96 h and prepared for surface potential tests and local AC impedance measurement. Surface potential tests were performed with a SKP electrochemical workstation (model SKP370) at approximately 20±2 ℃. The scanning mode is used with the step length of 150 μm, the probe vibration frequency of 80 Hz and the amplitude of 30 μm. LEIS measurement was carried out on a local electrochemical workstation (model LEIS370) at approximately 20±2 ℃. The scanning mode was applied with a step length of 150 μm, a probe vibration frequency of 10 Hz and an amplitude of 30 μm.

2.4. SEM observations and XRD and EDS analyses

The structure and corrosion morphology of the sample was observed using SEM. The compositional analysis for corrosion product was performed by energy dispersive spectroscopy (EDS) on the SEM instrument (model JSM6480LV). X-ray diffraction (XRD) was performed using a PHI Quantera SXM.

3. RESULTS AND DISCUSSION

3.1 The Al_2Cu intermetallic compound preparations and analysis

Fig. 2 shows the results of the analysis for the Al_2Cu intermetallic compound. The SEM image of intermetallic Al_2Cu contains some pits and cracks as shown in Fig. 2a, and the intermetallic Al_2Cu is very hard and brittle. Intermetallic Al_2Cu consists of only Al and Cu elements as shown by the EDS analysis results (Table 1). The mass percentage of the Al and Cu elements in intermetallic Al_2Cu is 45.6:54.4. Its atomic ratio is 66.4:33.6 and is close to 2:1. The diffraction peak of intermetallic Al_2Cu is consistent with the characteristic peaks of the theta (θ, Al_2Cu) phase (Fig. 2b).

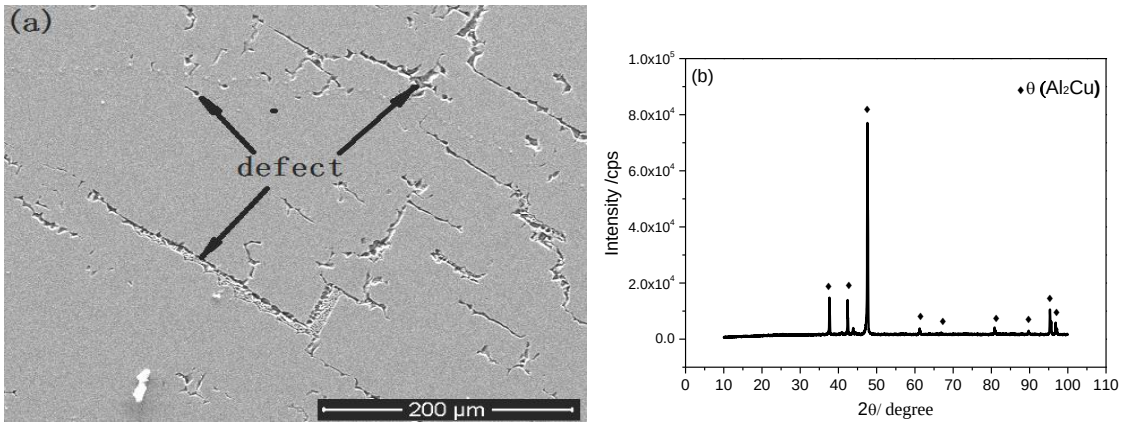

Figure 2. Analyses of intermetallic Al_2Cu (a) SEM image; (b) XRD analysis

Table 1. Chemical and atom composition of intermetallic Al_2Cu

Element	*Wt %*	A_t%
Al	45.6	66.4
Cu	54.4	33.6

3.2 Open circuit potential and potentiodynamic polarization curves analysis

Fig. 3 shows the polarization curves of intermetallic Al_2Cu and pure Al immersed in the 0.1 M Na_2SO_4 solution. Table 2 shows the free corrosion potentials (E_{corr}) and corrosion current densities (i_{corr}) calculated by the Tafel extrapolation method. The E_{corr} value of intermetallic Al_2Cu is approximately -473.04 mV (vs. SCE) and is higher than that for pure Al (about -507.16 mV (vs. SCE)). However, the i_{corr} value of intermetallic Al_2Cu in Table 2 is 0.77 μA higher than that of pure Al (approximately 0.22 μA) in 0.1 M Na_2SO_4 solution with pH 4.3.

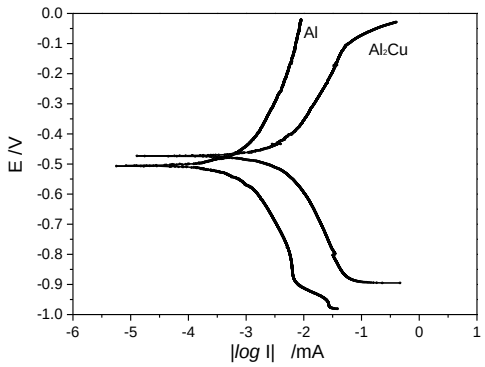

Figure 3. Polarization curves of Al_2Cu and pure Al in 0.1 M Na_2SO_4 solution

Table 2. Polarization curve fitting parameter value

Parameter	E_{corr} (V)	I_{corr} (μA)
Pure Al	-507.16	0.22
Al_2Cu (θ)	-473.04	0.77

3.3 AC impedance curve of intermetallic Al_2Cu

The EIS measurement of the samples as a function of time was carried out and the results are shown in Fig. 4. The Nyquist curves in Fig. 4a include an apparent capacitive semicircle in the high frequency region and one diffusion arc in the low frequency region between 1-8 h. Thus, one time constant is visible according to the Bode phase angle plots in Fig. 4b. However, one apparent capacitive semicircle is present, and two time constants are obtained from the Nyquist and phase plots

over the immersion time between 24-96 h. These EIS results suggest that the state of the surface of the Al_2Cu intermetallic compound electrode has been changed.

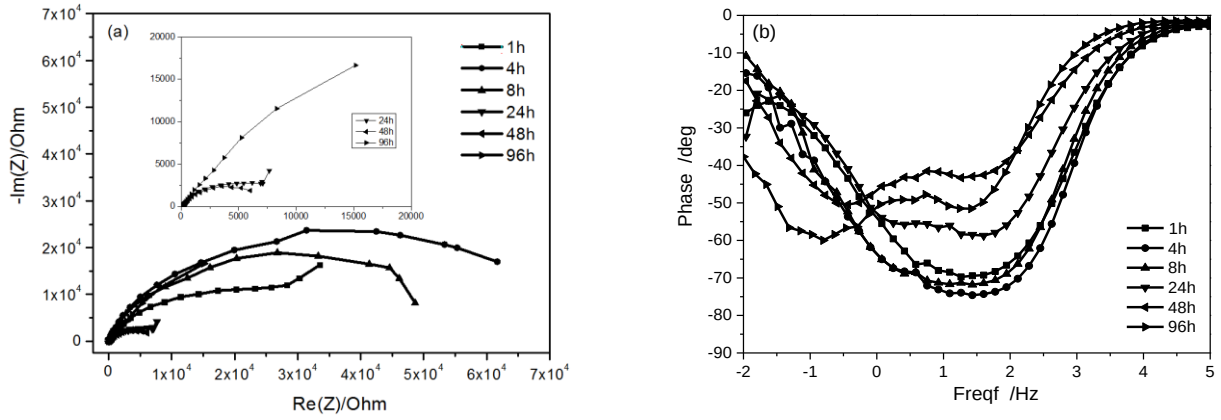

Figure 4. EIS plots of Al_2Cu with the increase of the immersion time (a) Nyquist plot; (b) bode plot

Figs. 5a and 5b show two equivalent circuits that were obtained by fitting the EIS spectra in Figs. 4a and 4b, respectively. Thin alumina films and corrosion products are present on the surface of the working electrode after long immersion. In the first equivalent circuit (Fig. 5a), R_s is the solution resistance, CPE is the double layer capacitance, and R_{ct} is the charge transfer resistance of the double layer. On the other hand, in the second equivalent circuit (Fig. 5b), R_s is the solution resistance, CPE1 is the outer layer capacitance including the passive film corrosion products, R_1 represents the resistance of the corrosion products, CPE2 represents the double layer capacitance of the anodic area, and R_{ct} corresponds to the charge transfer resistance of the double layer.

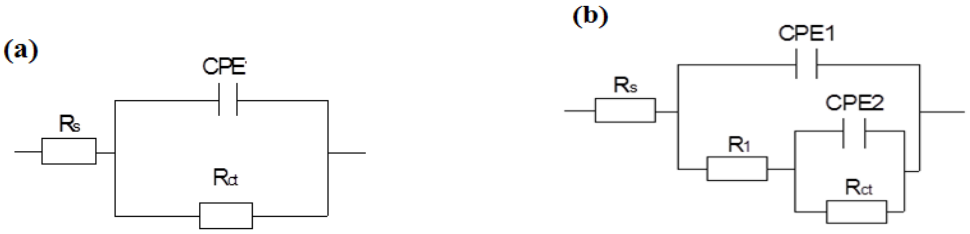

Figure 5. Equivalent circuits of Al_2Cu electrode surface (a) equivalent circuits over the immersion time between 2 and 8 h; (b) equivalent circuits over the immersion time between 24-96 h

The typical EIS parameters can be determine using the equivalent circuits and are listed in Tables 3 and 4. In the equivalent circuits (Figs. 5a and 5b), R_s is the solution resistance. It is obvious that the R_s value becomes stable during the immersion time as expected. The capacitance is replaced by the so-called constant phase angle element (CPE, $Z_{CPE} = 1/Y_0(jw)^n$, where Z_{CPE} is the impedance of the constant phase element ($\Omega.cm^2$), w is the angular frequency of ac-voltage (rad s^{-1}), and Y_0 and n are the frequency independent parameters). The presence of CPE has been often explained by dispersion

effects that can be caused by microscopic surface roughness [27, 28]. The value of $(Y_0)_1$ can be regarded as the value of the outer layer capacitance (CPE1) including the passive film and corrosion products. The value of $(Y_0)_2$ is thought to be an approximation of the double layer capacitance of the anodic area (CPE2). The values of *n* are usually related to the electrode surface roughness. For a perfectly smooth electrode, *n* will have a value of 1, and the impedance of a CPE will be equal to that of a pure capacitor. In corrosion studies, a low value of *n* can be ascribed to a roughening of the electrode due to corrosion. The rougher the electrode is, the lower the value of n becomes. This is because the real area of the corroded electrode is varied in the corrosion process, causing the deviation from smooth electrode [29].

Table 3. Parameters from EIS measurements over the immersion time between 2-8 h

Time	1 h	4 h	8 h
R_s, $\Omega \cdot cm^2$	27.66	26.71	30.97
$Y_{0,}\ \Omega^{-1}cm^{-2}S^{-n1}$	1.97E-5	2.298E-5	2.768E-5
n	0.8059	0.8343	0.8278
R_{ct}, $\Omega \cdot cm^2$	1.189E5	6.474E4	4.818E4

Table 4. Parameters from EIS measurements over the immersion time between 24-96 h

Time	24 h	48 h	96 h
R_s, $\Omega \cdot cm^2$	26.58	29.59	26.72
$(Y_0)_{1,}\ \Omega^{-1}cm^{-2}S^{-n1}$	5.039E-5	1.731 E-4	1.565 E-4
n_1	0.82	0.74	0.81
R_1, $\Omega \cdot cm^2$	852.2	424.5	568
$(Y_0)_{2,}\ \Omega^{-1}cm^{-2}S^{-n2}$	7.718E-5	3.19 E-4	3.022 E-4
n_2	0.62	0.76	0.81
R_{ct}, $\Omega \cdot cm^2$	1.033E4	6929	4.424E4

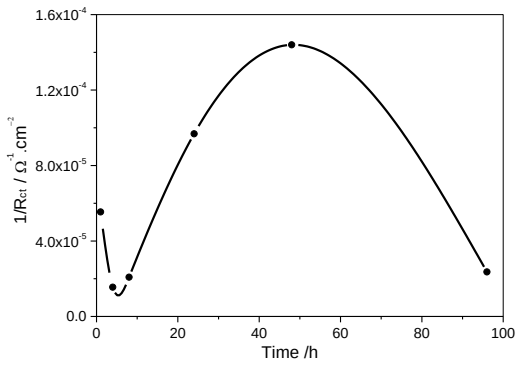

Figure 6. Variation of the corrosion rates of intermetallic Al_2Cu as a function of different immersion time

The reciprocal of the charge transfer resistance R_{ct} is used as a parameter to characterize the corrosion rate in this paper [30]. $1/R_{ct}$ Values for different immersion times are calculated from the medium frequency range as shown in Fig. 6. The corrosion rates vary with the immersion time. The corrosion rate of intermetallic Al_2Cu declines continuously in the initial stage of immersion (1-4 h), increasing during the immersion time of 4-48 h and decreasing gradually in the late stage of immersion (48-96 h). The highest corrosion rate is observed at 48 h.

3.4 Surface potential change of the coupled Al_2Cu/Al electrode

The line scan potential of the coupled Al_2Cu/Al electrode before and after the immersion is shown in Fig. 7. The Al_2Cu potential is higher than that of pure Al near the interface before the immersion (Fig. 7a) and this result is identical to the corrosion potential in Fig. 3. The potential of coupled Al_2Cu/Al at the interface is -0.651 V at 0 h and became -0.721 V after 96 h of immersion. The potential of the pure Al region remained stable before and after the immersion. However, the Al_2Cu potential value at the local area (dot A) increased significantly to approximately 0.384 V. The corrosion area of the coupled Al_2Cu/Al interface is close to the side of the pure Al expanded. The corrosion degree of coupled Al_2Cu/Al at the interface is aggravated after the immersion and after the pure Al is highly dissolved.

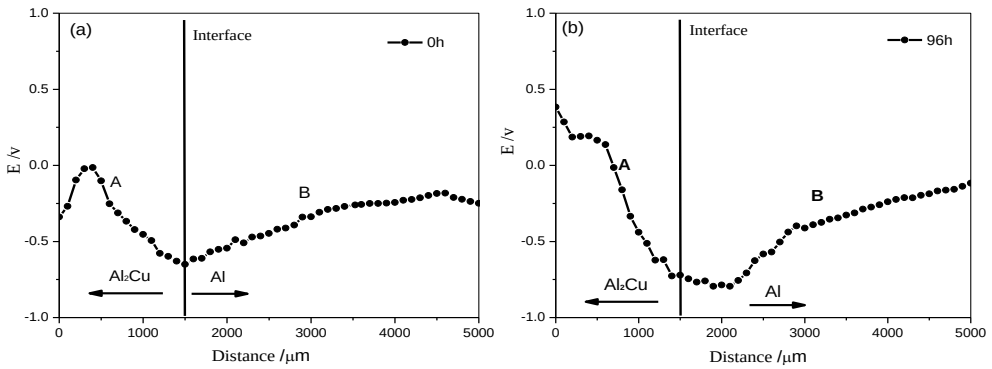

Figure 7. Potential of Al_2Cu/Al electrode before and after the immersion (a) 0 h; (b) 96 h

3.5 Local impedance change of Al_2Cu/Al electrode

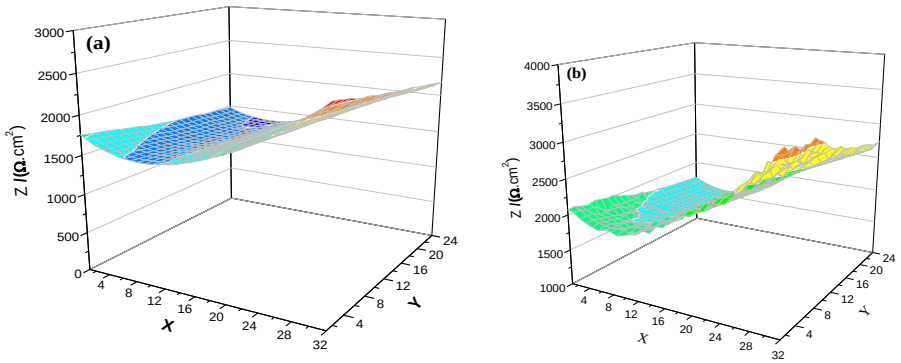

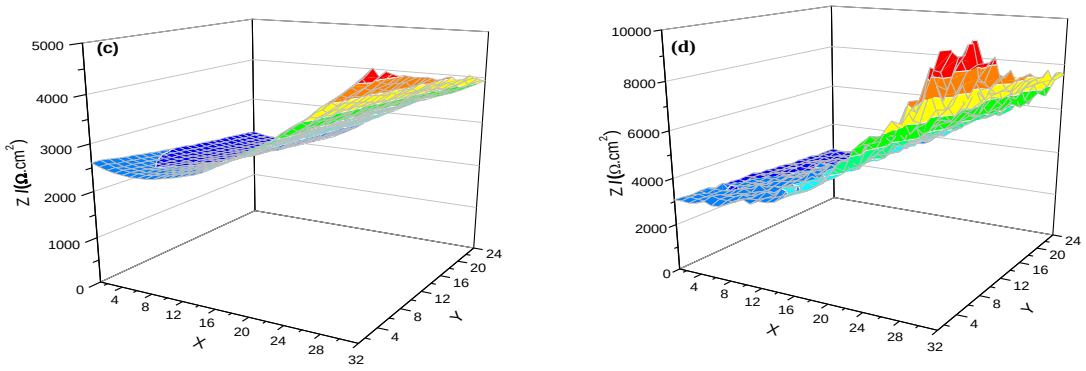

Figure 8. Local impedance values of Al_2Cu/Al electrode immersed for different time (a) 2 h; (b) 16 h; (c) 48 h; (d) 96 h

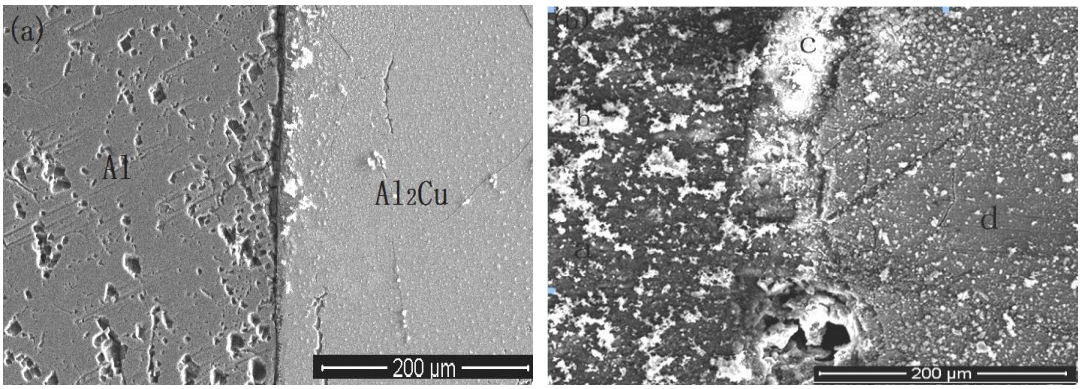

Figure 9. Surface image of coupled Al_2Cu/Al before and after immersion (a) 0 h; (b) 96 h

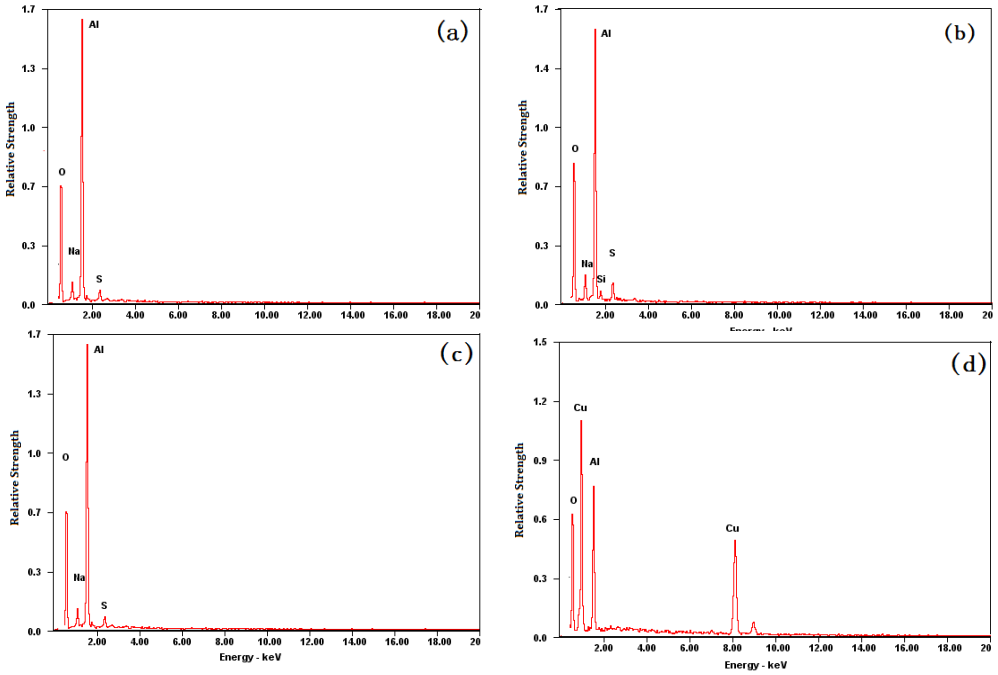

Figure 10. Energy spectrum of the corrosion products near the Al_2Cu/Al interface after the immersion (a) dot a; (b) dot b; (c) dot c; (d) dot d

Local impedance values of coupled Al_2Cu/Al immersed in solution for different time (scanning area 5 mm×5 mm) are shown in Fig. 8. The impedance values of pure Al vary from approximately 1700 $\Omega.m^2$ to 2500 $\Omega.m^2$ during the immersion. Meanwhile, the Al_2Cu impedance value increases greatly from approximately 2200 $\Omega.m^2$ to 7500 $\Omega.m^2$ and is higher than that of the pure Al. Therefore, the pure Al is dissolved easier than the Al_2Cu by the corrosion potential. This shows that the Al_2Cu region in coupled Al_2Cu/Al immersed in a solution is more difficult to dissolve relative to pure Al. This result is consistent with line scan potential and corrosion potential results.

The surface morphology of coupled Al_2Cu/Al before and after the immersion is shown in Fig. 9. The sample surface is covered with a few corrosion products as shown by the corrosion morphology observation in Fig. 9b. The corrosion products are uneven and thick in the local regions due to corrosion product accumulation. There are many corrosion pits and holes, and the pitting in the Al region is more severe than in the Al_2Cu region. The corrosion products in the Al region mainly contain Al, Na, O and S elements as shown from EDS analysis in Figs. 10a and 10b and Al, Cu, O and S elements in the Al_2Cu region as shown in Fig. 10d. However, corrosion products mainly contain Al, O and S elements in the coupled Al_2Cu/Al interface in Fig. 10c. The corrosion products are mainly Al oxide and Al sulfate [31].

3.6 Analyses and discussion

When intermetallic Al_2Cu or coupled Al_2Cu/Al is immersed in 0.1 M Na_2SO_4 acidic solution simulating an industrial pollution atmospheric environment, the reduction of oxygen and dissolution of Al mainly occurs. The surface dissolution reaction on the sample surface is as follows [22, 31]:

$$Al - 3e \rightarrow Al^{3+} \quad (1)$$

$$O_2 + 4H^+ + 4e \rightarrow 2H_2O \quad (2)$$

At the same time, the following reaction also occurred due to the weak acid environment:

$$H_2O \rightarrow H^+ + OH^- \quad (3)$$

$$Al^{3+} + 3OH^- \rightarrow Al(OH)_3 \quad (4)$$

$$Al(OH)_3 \rightarrow AlOOH + H_2O \text{ or } 2Al(OH)_3 \rightarrow Al_2O_3 + 3H_2O \quad (5)$$

$$Al_2O_3 + 6H^+ \rightarrow 2Al^{3+} + 3H_2O \quad (6)$$

$$2Al^{3+} + 3SO_4^{2-}(aq) + xH_2O \rightarrow Al_2(SO_4)_3 \cdot xH_2O \quad (7)$$

These reactions could explain the corrosion behavior of the intermetallic Al_2Cu or coupled Al_2Cu/Al sample surface. When intermetallic Al_2Cu or coupled Al_2Cu/Al is immersed in the solution, the dissolution of Al and Al oxide occurs primarily at the initial stage of the immersion. The Al oxide is dissolved and formed at the same time. The formation of Al oxide is the main results of the consumption of the hydrogen ions. Therefore, the Al oxide is the main corrosion product and covers the sample surface. A small amount of Al sulfate also appears among the Al oxide.

The potential of intermetallic Al_2Cu is approximately -473.04 mV in Fig. 3 and is similar to the potential in the 0.5 M H_2SO_4 solution [32]. This is different from the potential in the NaCl solution [22, 23]. The potential of pure Al is more negative than the potential of intermetallic Al_2Cu, and this is

in accordance with the previous result reported in the references [22, 23, 32]. Pure Al is more easily dissolved than intermetallic Al_2Cu in 0.1 M Na_2SO_4 solution according to thermodynamics analysis of the potential order. It appears that this is not completely correct if the dissolution of Al_2Cu appears faster than Al according to the I_{corr} values. The origin of this effect is related to the structural characteristics of intermetallic Al_2Cu and the selective dissolution of Al in intermetallic Al_2Cu [9].

The corrosion behavior of intermetallic Al_2Cu varies for 96 h in accordance with the impedance spectrum. Nyquist spectra (Fig. 3a) show one apparent capacitive semicircle and one diffusion arc at the time of 1 h. This phenomenon can be explained as follows: after the sample is immersed in 0.1 M Na_2SO_4 solution with pH 4.3, the oxidation film on the sample surface is in contact with the solution ions and then reacts with hydrogen ions. The hydrogen ion far away from the sample surface could transfer into the sample surface when hydrogen ion concentration near the sample surface decreases because of reaction consumption. This indicates that the reaction on the double layer surface is controlled with the diffusion of the hydrogen ion and the Nyquist spectra curve of low frequency is the diffusion arc. When the sample is immersed in solution for approximately 4 hours, the diffusion of hydrogen ions is not the primary factor. Therefore, the low frequency diffusion arc disappears (Fig. 3b) and the corrosion rate on the sample surface decreases. The reaction between the hydroxyl ion and Al primarily occurs on the sample surface due to the consumption of hydrogen ions from 1 h to 8 h. The anodic reaction is the reduction of Al and the cathodic reaction is the oxidation of oxygen. The corrosion rate on the sample surface increases. There is one apparent capacitive semicircle and two time constants obtained from the Nyquist spectra curve and Bode phase angle plots of 24-48 h of immersion. This means that the corrosion products of Al, e.g., Al oxide and Al sulfate, are deposited on the sample surface and change the structure of the double electric layer on the surface. At this time, because there is only a small amount of the corrosion product, the anodic reaction and cathodic reaction on the surface are influenced less. The corrosion rate increases. With the increase of the immersion time, the thickness of the corrosion products increases due to the rising amount of the corrosion product; this hinders the dissolution of Al and the diffusion of hydrogen and oxygen. Therefore, the corrosion rate on the sample surface decreases again.

When the coupled Al_2Cu/Al electrode is immersed in solution, the pure Al and Al_2Cu in the coupled Al_2Cu/Al electrode are dissolved. However, Al_2Cu and Al in the vicinity of the coupled Al_2Cu/Al interface have different potentials (Fig. 3), giving rise to galvanic corrosion. The galvanic corrosion of the coupled Al_2Cu/Al interface induces the strong dissolution of pure Al, while intermetallic Al_2Cu is protected as a cathode because the potential of the pure Al is more negative than that of intermetallic Al_2Cu. This result is similar to the potential analysis of Al_2Cu particle in Al-10 wt.% Si-3 wt.% Cu alloy, where the Volta potential map is between +350 mV and +450 mV relative to the matrix as found by scanning Kelvin probe force microscopy (SKPEM) [19]. The galvanic corrosion results in coupled Al_2Cu/Al are the current density results of the coupled Al_2Cu and Al in 0.005 M NaCl [25] and the micro-current values between IMP and Al [24], confirming that Al served as an anode, involving the dissolution of aluminum as described by Eq. (1), and Al_2Cu served as a cathode, involving the reduction of dissolved oxygen. The amount of corrosion product at the coupled Al_2Cu/Al interface increases (Fig. 9b). This result is identical to the local impedance value. The local impedance value of intermetallic Al_2Cu in coupled Al_2Cu/Al increases over the immersion time, and

pure Al local impedance remains stable. Simultaneously, the dissolution of Al or Al_2Cu far from the coupled Al_2Cu/Al interface continued. Therefore, while some corrosion products are present on the Al or Al_2Cu surface [25], their amount is smaller than that at the coupled Al_2Cu/Al interface. The corrosion degree on the coupled Al_2Cu/Al interface is more serious than at the Al_2Cu intermetallic compound or pure Al surface (Fig. 9b). Therefore, coupled Al_2Cu/Al promotes localized corrosion of the 2A12 alloy.

4. CONCLUSIONS

The mass percentage of Al and Cu elements for intermetallic Al_2Cu is 45.6:54.4, and its atomic ratio is 66.4:33.6. The corrosion potential of intermetallic Al_2Cu is approximately -473.04 mV and is higher than that of pure Al in 0.1 M Na_2SO_4 solution with pH 4.3. The EIS results for intermetallic Al_2Cu reveal that the highest corrosion rate over the immersing time between 0 and 96 h is observed at 48 h. The potential of intermetallic Al_2Cu is higher than that of pure Al near the interface as obtained by the scan potential of coupled Al_2Cu/Al. Local impedance results of coupled Al_2Cu/Al indicate that the local impedance of intermetallic Al_2Cu increases greatly from approximately 2200 $\Omega.m^2$ to 7500 $\Omega.m^2$ and is greater than that of pure Al. To summarize, the corrosion mechanism of coupled Al_2Cu/Al is such that pure Al is highly dissolved and acts as the anode and intermetallic Al_2Cu is protected as the cathode because of the galvanic corrosion of coupled Al_2Cu/Al.

ACKNOWLEDGEMENTS
The authors gratefully acknowledge the support of the National Natural Science Foundation of China (No. 50971048) and national material environmental corrosion platform. In addition, many thanks are due to Dr. W. L Wang for the assistance with the SKP and LEIS measurements.

References

1. J. Zhang, Y. N. Huang, C. Mao, P. Peng, *Solid State Commun.*, 152 (2012) 2100
2. K. K. Babu, K. Panneerselvam, P. Sathiya, A. N. Haq, S. Sundarrajan, P. Mastanaiah, C.V. S Murthy, *Mater. Today: Proceedings*, 4 (2017) 285
3. S. C. Wang, M. J. Starink, N. Gao, *Script. Mater.*, 54 (2006) 287.
4. J. A. Derose, T. Suter, A. Bałkowiec, J. Michalski, K. J. Kurzydlowski, P. Schmutz, *Corros. Sci*., 55 (2012) 313
5. M. B. Lahovary, L. Laffont, C. Blanc, *Corros. Sci*., 119 (2017) 60
6. N. Birbilis, Y. M. Zhu, S. K. Kairy, M. A. Glenn, J. F. Nie, A. J. Morton,Y. G. Garcia, H. Terryn, J. M. C. Mol, A. E. Hughes, *Corros. Sci*., 113 (2016) 16
7. C. Senoz, S. Borodin, M. Stratmann, M. Rohwerder, *Corros. Sci*., 58 (2012) 307
8. C. Blanc, A. Freulon, M. C. Lafont, Y. Kihn, G. Mankowski, *Corros. Sci*., 48(2006) 3838
9. N. Birbilis, M. K. Cavanaugh, R. G Buchheit, *Corros. Sci*., 48(2006) 4202
10. F. M. Queiroz, M. Magnani, I. Costa, H. G. Melo, *Corros. Sci*., 50(2008)2646
11. R. Ambat, A. J. Davenport, G. M. Samans, A. Afsth, *Corros. Sci*., 48(2006) 3455
12. X. Zhang, T. Hashimoto, J. Lindsay, X. Zhou. *Corros. Sci*., 108 (2016) 85
13. F.Eckermann, T. Suter, P.J. Uggowitzer, A. Afseth, P. Schmutz, *Electrochim. Acta*, 54(2008) 844
14. S. Dey, M.K. Gunjan, I. Chattoraj, *Corros. Sci*., 50(2008) 2895
15. W. D. Ren, J. F. Li, Z. Q. Zheng, W. J. Chen,*Trans. Nonferrous Met. SOC. China*, 17(2007)727

16. A. C. Vieira, A. M. Pinto, L. A. Rocha, S. Mischlerb, *Electrochim. Acta*, 56(2011)3821
17. C. Mondal, A. K. Mukhopadhyay, *Mater. Sci. Eng., A*, 391(2005)367
18. M. Voncina, J. Medved, T. Boncina, F. Zupani. *Trans. Nonferrous Met. Soc. China*, 24(2014) 36
19. L.E. Fratila-Apachitei, I. Apachitei, J. Duszczyk, *Electrochim. Acta*, 51 (2006) 5892–5896
20. M. Chopka, S. Kumar, D. R. Bhandari, P K Das, I Manna, *Mater. Sci. Eng., B*, 139(2007)141
21. W. R. Osorio, J. E. Spinelli, C. M. A. Freire, M. B. Cardona, A. Garcia, *J. Alloys Compd.*, 443(2007) 87
22. D. Song, A. B. Ma, J. H. Jiang, P. H. Lin, L. Y. Zhang, *Prog Nat. Sci.: Mater. Int.*, 21(2011)307
23. J. F. Li, Z. Q. Zheng, N. Jiang, C. Y. Tan, *Mater. Chem. Phys*., 91(2005)325
24. L. T. Yin, Y. Jin, C. Leygraf, J. S. Pan. *Electrochim. Acta*, 192 (2016) 310
25. H. W. Shi, E. H. Han, F. C. Liu, T. Wei, Z. W. Zhu, D. K. Xu. *Corros. Sci*., 98 (2015) 150
26. H. N. Krogstad, R. Johnsen, *Corros. Sci*., 121 (2017) 43
27. J. Xu, C. Z. Zhuo, D. Z. Han, J. Tao, L. L. Liu, S. Y. Jiang, *Corros. Sci*., 51(2009)1055
28. Z. Zhang, J. Q. Zhang, J. M. Wang, C. N. Cao, *Trans. Nonferrous Met. Soc. China*, 11(2001) 284
29. E. B. Castro, C. A. Gervasi, *Int. J. Hydrogen Energy*, 25(2000) 1163
30. H. R. Zhou, X. G. LI, J. Ma, C. F. Dong, *Mater. Sci. Eng., B*, 162(2009) 1
31. T. E. Graedel, *J. Electrochem.Soc.*, 136(1989)204c
32. W. B. R. Osorio, J. E. Spinelli, I. L. Ferreira, A. Garcia, *Electrochim. Acta*, 52 (2007) 3265